

## 水基超材料宽带大功率微波吸波器

邓光晟<sup>1,2\*</sup>, 陈文卿<sup>1</sup>, 余振春<sup>1,2</sup>, 杨军<sup>1,2</sup>, 尹治平<sup>1,2</sup><sup>1</sup>合肥工业大学光电技术研究院特种显示与成像技术安徽省技术创新中心, 安徽 合肥 230009;<sup>2</sup>合肥工业大学仪器科学与光电工程学院测量理论与精密仪器安徽省重点实验室, 安徽 合肥 230009

**摘要** 设计了一种基于介质谐振器的水基微波吸波器。介质谐振器包括两个长方体介质板和一个十字形空腔,并在其内部充满水以实现宽带微波吸收效果。不同于传统水基超材料中相互独立的水基单元,本设计中十字形空腔所形成的水流通道横截面面积达到  $3\text{ mm} \times 3\text{ mm}$ ,可确保阵列中水流畅通,因此该结构满足水冷工作要求,可实现大功率微波的无衰减吸收。仿真结果表明,在  $21.8 \sim 35.9\text{ GHz}$  的微波频段内,吸波器对入射电磁波的吸收率大于  $90\%$ ,相对吸收带宽为  $48.9\%$ 。此外,该吸波器对入射波的偏振不敏感,在宽频段范围内对大入射角电磁波仍有高吸收效果。通过 3D 打印技术实现了样品加工,实验结果与模拟结果吻合良好。该吸波器在宽带大功率微波吸收领域有较大的应用潜力。

**关键词** 材料; 超材料; 吸波器; 宽带; 大功率; 水基介质

**中图分类号** O436 **文献标志码** A

**DOI:** 10.3788/CJL202249.2103001

## 1 引言

宽带吸收是微波吸收体的一个重要特性,在雷达隐身<sup>[1]</sup>、反电磁干扰<sup>[2]</sup>以及传感<sup>[3]</sup>等领域中均有良好的应用价值,受到了广泛的关注。微波吸收器可以通过单元设计定制其电磁特性,进而实现宽带吸收<sup>[4-6]</sup>。同时,研究人员提出了各种方法来扩展微波吸收器的带宽,包括多层设计<sup>[7-10]</sup>、基于电阻膜的多层结构<sup>[11]</sup>、具有多个谐振器的超级单元<sup>[12]</sup>和高阻抗表面<sup>[13-14]</sup>。然而,由此带来的设计和制造的复杂性以及加工成本也不可避免地增加了。近年来,由传统微波吸收材料组成的全介质超材料吸收器在改善宽频带阻抗匹配方面显示出其独特的潜力,可以通过改变这些吸收器的特定结构来有效地调节它们的阻抗。研究人员利用这些全介质材料构建了宽带吸收器<sup>[15-16]</sup>。全介质吸波器的电磁特性对于波吸收而言是至关重要的。水作为地球上丰富的自然资源,具有高介电常数<sup>[17]</sup>和高频色散<sup>[18]</sup>,在全介质吸波器中的应用具有明显的优势<sup>[19]</sup>。此外,水具有相对较高的介电损耗,是宽带吸收的理想材料。由于水的流动性,可以通过设计水基吸收器的结构,在更宽的频率范围内实现吸波器与背景的阻抗匹配。在这种情况下,介质腔就像一个容器,而充满的高介电损耗的水在吸收入射电磁波方面起着关键的作

用。Zhao 等<sup>[20]</sup>提出了一种水滴结构的微波吸波器,在  $7.5 \sim 15\text{ GHz}$  范围内实现了吸收率为  $90\%$  的微波吸收。Chen 等<sup>[21]</sup>提出了一种基于纯水的微波吸波器,该吸波器呈十字交叉立体状,可在  $8 \sim 20\text{ GHz}$  范围内实现吸收率为  $90\%$  的吸收。Pang 等<sup>[22]</sup>提出了一种水基微波吸波器,在  $6.4 \sim 30\text{ GHz}$  范围内实现了吸收率为  $90\%$  的吸收,且该吸波器对横电(TE)波和横磁(TM)波都具有广角吸收性能。Xiong 等<sup>[23]</sup>设计了一种盐水基微波吸波器,在  $1.4 \sim 3.3\text{ GHz}$  和  $4.3 \sim 63\text{ GHz}$  的频带内,其吸收率大于  $90\%$ ,并且可以通过改变盐度来调节吸收性能。Zhang 等<sup>[24]</sup>提出了一种十字形状的水基超宽带微波吸波器,该吸波器在  $9.3 \sim 49.0\text{ GHz}$  频段的吸收率大于  $90\%$ ,每个单元四个面各有一个水流通道连接相邻单元。Lu 等<sup>[25]</sup>开发了以氧化铟锡(ITO)薄膜为衬底的两层周期性排列的水柱,在  $4.6 \sim 33.7\text{ GHz}$  和  $51 \sim 83\text{ GHz}$  的吸收波段,吸收率均大于  $90\%$ ,具有广角吸收性能。Yoo 等<sup>[26]</sup>设计了一种水滴结构的超材料吸波器,通过改变水滴的形状和尺寸,可实现吸收带宽和吸收率的调节。尽管上述水基微波吸波器都表现出宽带吸收性能,但大多吸波器的单元独立,水溶液不流通,或是相邻单元的水流通道截面积太小,水流流通困难。由于水基超材料吸收的微波能量大部分转化为水的热

收稿日期: 2022-01-19; 修回日期: 2022-02-18; 录用日期: 2022-03-08

基金项目: 国家自然科学基金(61871171)、航空科学基金(2020Z0560P4001)、中央高校基本科研业务费资助项目(JD2020JGPY0012)

通信作者: \*dgsh@hfut.edu.cn

量,若水体本身不能流通散热,积聚的热量会严重恶化吸波器的工作性能。可设计一种水流通道截面积较大的水基谐振单元,使水溶液内外循环以带走吸波体工作时产生的热量,从而满足大功率微波吸收的需求。

本文设计了一种可实现宽带电磁波吸收的水基超材料吸波器。相比传统的水基吸波超材料,该结构中十字形空腔所形成的水流通道横截面面积达到  $3\text{ mm} \times 3\text{ mm}$ ,可满足吸波器的水冷工作要求,从而实现大功率微波的高效吸收。模拟结果表明,该吸波器在  $21.8 \sim 35.9\text{ GHz}$  的频率范围内可以保持  $90\%$  以上入射波吸收率,相对吸收带宽为  $48.9\%$ 。所提出的结构对入射波的极化不敏感,且对  $45^\circ$  入射的电磁波仍能在宽频带内保持  $85\%$  以上的吸收率。此外,仿真分析发现,该结构对水温的变化不敏感,这对大功率微波吸收是非常重要的。利用 3D 打印技术加工了样品,实验结果证实该结构具有良好的宽带、广角电磁波吸收能力。

## 2 结构设计与加工

### 2.1 结构模型

该水基超材料吸波器由介质谐振腔和铜基底构成。图 1 给出了水基谐振单元的示意图,介质谐振腔为十字形空腔,具有储水的功能,且起到水流内部流通通道的作用。介质层厚度与空腔截面积的设计原则为加工后的阵列样品不易破裂且空腔截面积尽可能大。此外,还需兼顾吸波器在宽频带范围内满足入射波的阻抗匹配。谐振单元底部覆上一层铜板以阻止入射电磁波透过。为了方便吸波器的 3D 打印制备,超材料介质层选用的材料为树脂,其相对介电常数为  $2.9$ ,损耗正切为  $0.02$ 。在室温条件下获得的超材料吸波器的最佳尺寸参数为:上层介质基板厚度  $H_1 = 1.4\text{ mm}$ ,水腔厚度  $H_2 = 3\text{ mm}$ ,下层介质基板厚度  $H_3 = 1.4\text{ mm}$ ,内部介质层宽度  $W_1 = 1.5\text{ mm}$ ,水腔连通口宽度  $W_2 = 3\text{ mm}$ ,单元周期长度  $P = 6\text{ mm}$ 。

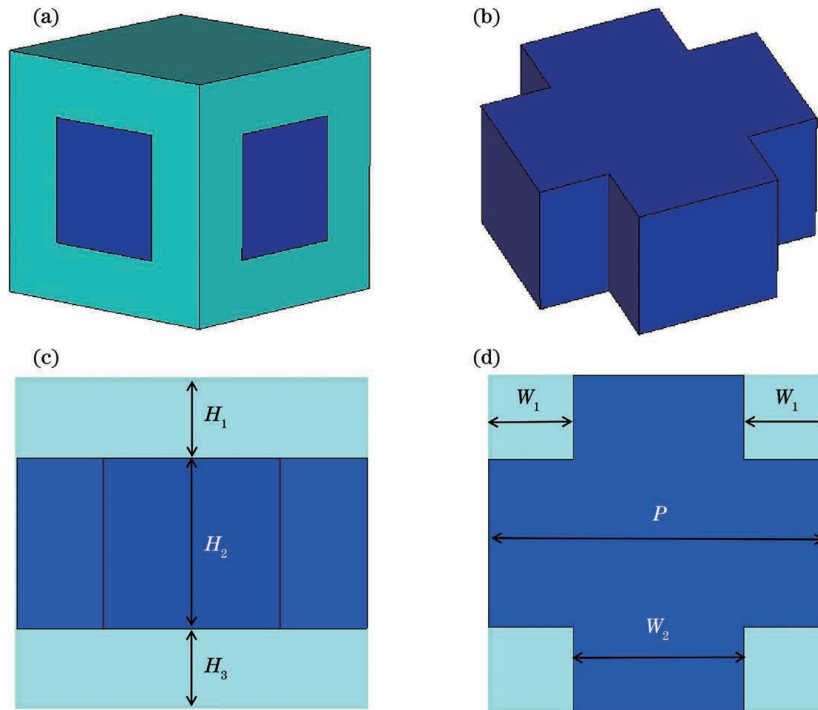


图 1 水基超材料吸收器示意图。(a)单元结构;(b)水腔示意图;(c)单元侧视图;(d)单元俯视图

Fig. 1 Schematics of absorber based on water-based metamaterial. (a) Unit structure; (b) diagram of water cavity; (c) side view of unit; (d) top view of unit

仿真中使用 Debye 模型来描述水在不同频率( $\omega$ )和不同温度( $T$ )下的介电常数<sup>[27]</sup>:

$$\epsilon(\omega, T) = \epsilon_0(T) + \frac{\epsilon_\infty(T) - \epsilon_0(T)}{1 - i\omega\tau(T)}, \quad (1)$$

式中: $\epsilon_\infty$ 和 $\epsilon_0$ 分别为水的高频介电常数和静态介电常数; $\tau$ 为旋转弛豫时间。这三个参数与水的温度 $T$ 的关系<sup>[28]</sup>为

$$\epsilon_0(T) = a_1 - b_1 T + c_1 T^2 - d_1 T^3, \quad (2)$$

$$\epsilon_\infty(T) = \epsilon_0(T) - a_2 \exp(-b_2 T), \quad (3)$$

$$\tau(T) = c_2 \exp\left(\frac{d_2}{T + T_0}\right), \quad (4)$$

式中: $a_1 = 87.9$ ;  $b_1 = 0.404\text{ }^\circ\text{C}^{-1}$ ;  $c_1 = 9.59 \times 10^{-4}\text{ }^\circ\text{C}^{-2}$ ;  $d_1 = 1.33 \times 10^{-6}\text{ }^\circ\text{C}^{-3}$ ;  $a_2 = 80.7$ ;  $b_2 = 4.42 \times 10^{-3}\text{ }^\circ\text{C}^{-1}$ ;  $c_2 = 1.37 \times 10^{-13}\text{ s}$ ;  $d_2 = 651\text{ }^\circ\text{C}$ ;  $T_0 = 133\text{ }^\circ\text{C}$ 。

### 2.2 样品加工与测试

采用打印机完成了  $25 \times 25$  单元阵列的超材料吸波器的加工制备,所得样品如图 2(a)所示。在打印过

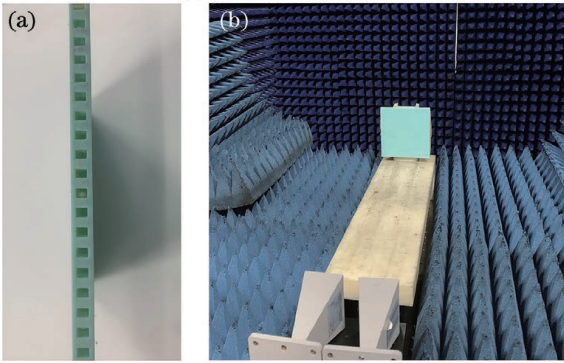


图 2 样品加工与测试。(a)样品;(b)实验平台

Fig. 2 Fabrication and measurement of sample. (a) Sample; (b) experiment platform

程中,打印机的两个喷头同时喷出分别用于构造外壳和空腔的固体复合树脂和水溶性树脂,并利用紫外光快速固化树脂材料。最后,溶解水溶性树脂以形成空腔,并注入水以填充空腔。样品测试在室温(25 °C)下进行,实验环境如图 2(b)所示。实验中,两个与矢量网络分析仪相连的喇叭天线分别作为发射端和接收端,调整样品位置使之与喇叭天线保持齐平。首先在待测样品位置放置与样品大小相同的铜板进行反射系

数( $S_{11}$ )的背景值测试,再将铜板替换为待测样品并测试样品的  $S_{11}$  值,将其与背景值相减,就可以得到待测样品的真实反射系数。吸波器的吸收率( $A$ )可根据测得的反射系数  $S_{11}$  求得:

$$A(\omega) = 1 - |S_{11}(\omega)|^2. \quad (5)$$

利用有限元方法(FEM)对吸波器的频谱曲线进行了模拟分析。在仿真中,在超材料单元四周的水流通道方向设置周期性边界条件,而垂直于介质基板的方向是电磁波的入射方向,在此设置开放边界用以模拟电磁波的传播。图 3(a)、(b)分别给出了模拟和测试得到的反射率曲线和吸收率曲线。在电磁波垂直入射的情况下,模拟得到的吸波器反射率在 21.8 ~ 35.9 GHz 的频率范围内低于 -10 dB,这也意味着吸波器在该频段内对入射波的吸收率大于 90%。我们定义相对吸收带宽为

$$R_B = 2 \frac{f_h - f_l}{f_h + f_l}, \quad (6)$$

式中: $f_h$  和  $f_l$  表示吸收率大于 90% 的频率范围的上限和下限。根据式(6),该吸波器的相对吸收带宽为 48.9%。从图 3 可以看出,测试结果与模拟结果吻合较好。

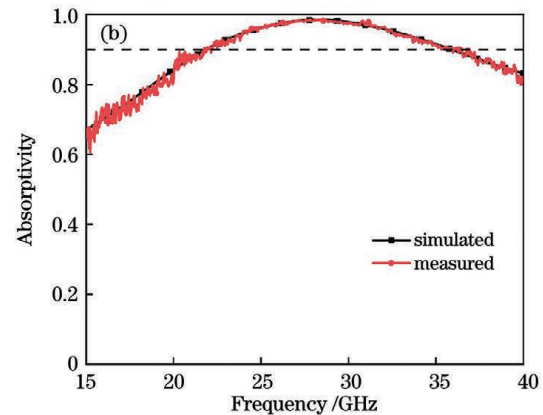
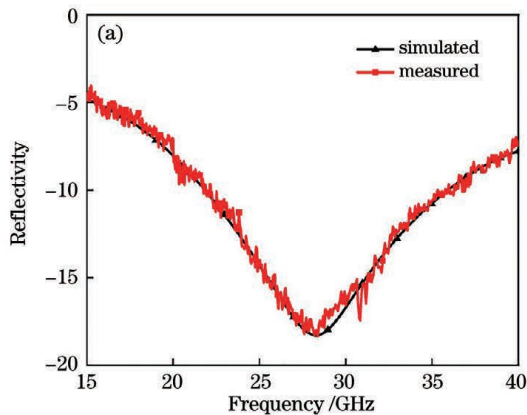


图 3 反射与吸收频谱图。(a)模拟与测试的反射频谱;(b)模拟与测试的吸收频谱

Fig. 3 Spectra of reflection and absorption. (a) Simulated and measured reflectance spectra; (b) simulated and measured absorption spectra

吸波器的宽带吸收机理可以用阻抗匹配原理来解释。对于超材料吸波器,其等效阻抗<sup>[29]</sup>可表示为

$$Z = \sqrt{\frac{(1 + S_{11})^2 - S_{21}^2}{(1 - S_{11})^2 - S_{21}^2}}, \quad (7)$$

式中: $S_{11}$  和  $S_{21}$  为分别为超材料吸波器的反射系数和透射系数。

当满足阻抗匹配条件时( $Z=1$ ),入射电磁波可以无反射地进入吸波器内部。利用模拟获得的  $S_{11}$  和  $S_{21}$  参数,计算得到的该水基超材料的等效阻抗随频率的变化曲线如图 4 所示。可以看出,在 21.8 ~ 35.9 GHz 的频段范围内,等效阻抗的实部和虚部基本保持在 1 和 0 附近,这有利于吸波器在工作频带内对入射波的高效吸收。

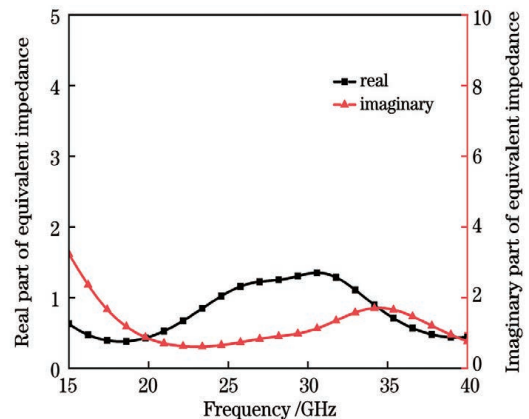


图 4 吸波器的等效阻抗

Fig. 4 Equivalent impedance of absorber

### 3 吸波特性和测试

为了分析宽带吸收的机理,模拟了峰值吸收频率处的水基超材料吸波器内部的电场、磁场以及功率损耗密度分布,模拟结果如图 5 所示。从图 5(a)、(b)所示的电场和磁场分布图可以看出,在水层周围和上层树脂板中存在较强的电场分布,同样位置也存在较强的环形磁场分布。说明该频率下的共振主要发生在水腔边界处与上层树脂板中,该谐振模式由电谐振和磁

谐振共同决定。根据功率损耗分布[图 5(c)]可以看出,电磁能量主要耗散于十字型水腔内部,尤其是单元连接通道的上侧区域,这与电场、磁场的位置一致,即在电磁场较强的区域产生了强烈的共振吸收。同时,虽然在上层树脂板中也存在较强的局域电磁场,由于水的高介电损耗特性,绝大部分的功率损耗仍集中在水层,证明了该吸波器中的水层是主要的吸波介质。虽然水腔中的下部及介质层内的功率损耗相对较小,但这部分结构为宽频段内的阻抗匹配提供了重要支撑。

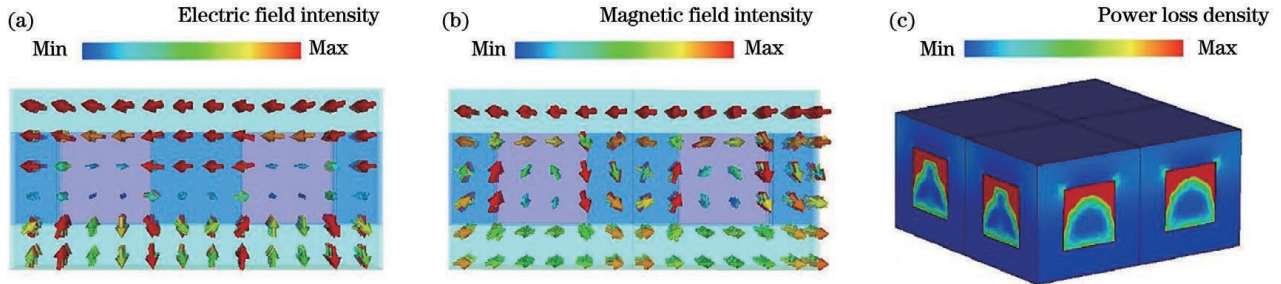


图 5 水基超材料吸波器在峰值吸收频率(28.28 GHz)处的场分布图。(a)电场分布;(b)磁场分布;(c)功率损耗密度分布  
Fig. 5 Field distributions of water-based metamaterial absorber at peak absorption frequency of 28.28 GHz. (a) Electric field distribution; (b) magnetic field distribution; (c) power loss density distribution

为了进一步研究结构与介质参数对吸收性能的影响,模拟计算了吸收率与不同的树脂基板厚度间的关系曲线。如图 6 所示,当上下介质基板的厚度从 0.5 mm 变化到 2 mm 时,超材料吸波器的吸收带宽和吸收率呈现出先增大后减小的趋势,其原因在于基板厚度变化后,超材料的等效阻抗也会改变。

对于所设计的结构而言,当基板厚度为 1.4 mm 时,超材料单元与入射波在宽频带内有最佳的阻抗匹配,表现出良好的宽带吸收效果。此外,除去水层之后,吸波器的吸收率大幅降低,这也进一步证明了该结构的宽带吸收主要来自于水对电磁波的吸收损耗。

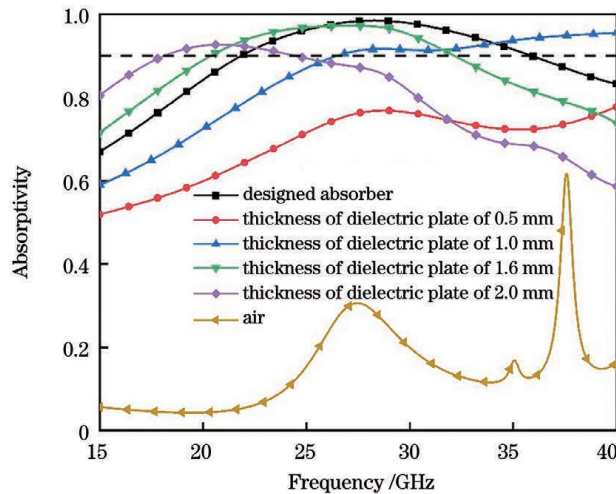


图 6 不同材料参数下的吸收频谱  
Fig. 6 Absorption spectra under different material parameters

在水基超材料吸波器中,水层对吸收带宽和吸收率有重要的影响。图 7(a)给出了内部介质层宽度  $W_1$  对吸收频谱的影响。当  $W_1$  增大时,结构单元中水腔的体积占比减小。由于水的介电常数大于介质的介电常数,此时谐振频率会发生红移,因此宽带吸收向低频端移动。当  $W_1$  为 1.5 mm 时,吸波器与入射波在宽频段内有最好的阻抗匹配。为了研究该结构中水流通

道大小对吸收率的影响,分别模拟了通道横截面积 ( $H_2 \times W_2$ ) 为 2 mm  $\times$  2 mm、3 mm  $\times$  3 mm 以及 4 mm  $\times$  4 mm 时的入射波吸收率,结果如图 7(b)所示。可以发现,当通道横截面积减小为 2 mm  $\times$  2 mm 时,吸波器的吸收带宽和吸收率均获得了一定的提升。进一步缩小通道的横截面积可以实现更好的吸收效果,但过小的通道横截面积不利于水流的循环和散热。

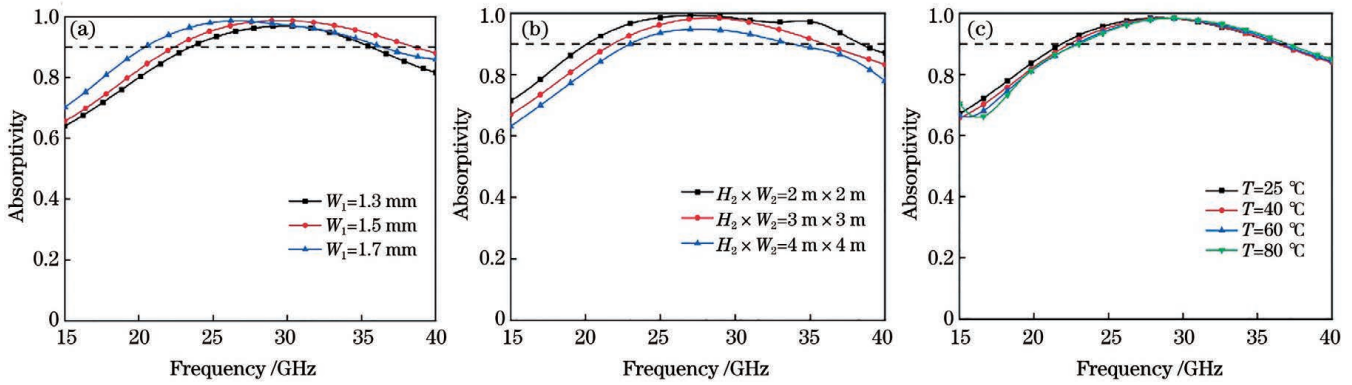


图 7 结构与材料参数对吸波器吸收频谱的影响。(a)内部介质层宽度;(b)水腔横截面积;(c)水温

Fig. 7 Influence of structure and material parameters on absorption spectra of absorber. (a) Width of internal medium layer; (b) cross-sectional area of water cavity; (c) water temperature

同样,当通道横截面积增大为  $4 \text{ mm} \times 4 \text{ mm}$  时,超材料的吸收带宽和吸收率会降低。综合考虑吸收性能和大功率微波吸收器对水冷效果的要求,最终选取的水流通道横截面积为  $3 \text{ mm} \times 3 \text{ mm}$ 。由于该水基吸波器吸收的电磁能量绝大部分转化为了水的热量,大功率的微波吸收会使得吸波器内的水温迅速增加。考虑到水的介电常数会受到温度的影响,模拟了不同水温下该吸收器的吸收性能,结果如图 7(c)所示。可以看出,随着温度的升高,吸收频段仅在低频端产生了微小的蓝移。当水温从  $25 \text{ }^\circ\text{C}$  变化到  $80 \text{ }^\circ\text{C}$  时,吸波器的相对吸收带宽的变化很小。可以认为,该结构的吸收性能对水温的依赖性很弱,这对大功率微波吸收是至

重要的。

对于超材料吸波器,一般希望其吸收性能不受入射波极化特性的影响,即对任意极化角的电磁波都能实现高效吸收。由于谐振结构的对称性,仅对极化角( $\varphi$ )为  $0^\circ \sim 45^\circ$  的吸收曲线进行了研究。图 8(a)所示的模拟结果表明,该水基吸波器对不同极化角的入射波具有完全相同的吸收特性。在  $21.8 \sim 35.9 \text{ GHz}$  的吸收频段范围内,吸收率始终保持在  $90\%$  以上,因此所设计的吸波器对入射波的极化角不敏感。此外,通过旋转样品,对其在不同极化条件下的吸收曲线进行了实验研究。如图 8(b)所示,测试结果证实了该吸波器结构的吸收性能与入射波极化特性无关。

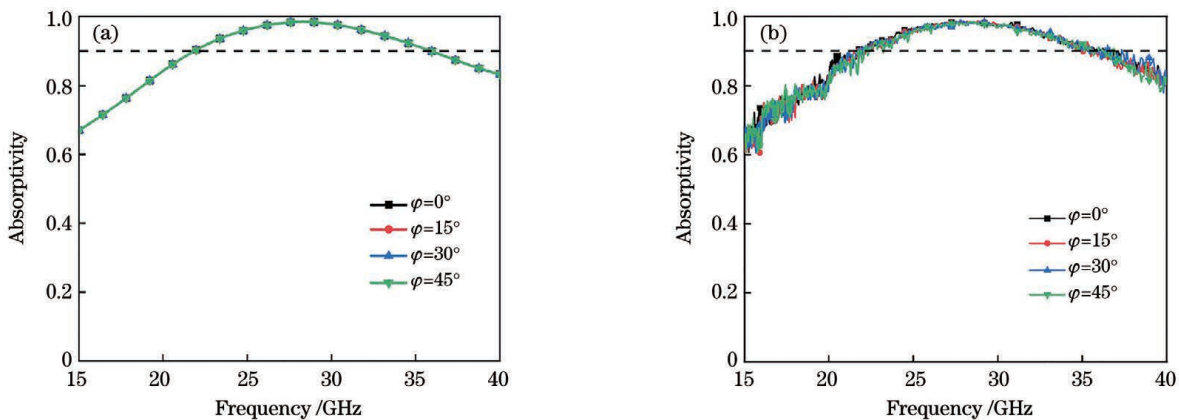


图 8 极化角对吸波体吸收频谱的影响。(a)模拟结果;(b)测试结果

Fig. 8 Effect of polarization angle on absorption spectrum of absorber. (a) Simulated results; (b) test results

最后,进一步考察了该吸波器对斜入射电磁波的吸收性能。图 9(a)给出了 TE 极化时不同入射角下的模拟得到的吸收曲线。当电磁波入射角( $\theta$ )小于  $30^\circ$  时,吸波器的吸收带宽与吸收率基本保持不变。当  $\theta$  达到  $45^\circ$  时,吸收频段的低频端和高频端均呈现出一定程度的蓝移,但仍可在  $23.7 \sim 37.3 \text{ GHz}$  频带范围内保持  $90\%$  以上的电磁波吸收率。测试得到的吸波器对不同入射角的 TE 极化波的吸收曲线如图 9(b)所示,可以看出,测试结果与模拟结果吻合较好。

图 10 给出了模拟和测试得到的 TM 极化时不同入射角下的吸收频谱曲线。随着  $\theta$  的增大,超材料吸波器的峰值吸收率略有下降,但吸收带宽增大,主要表现在上吸收频率会进一步向高频端移动。当  $\theta$  达到  $30^\circ$  时,在  $22.3 \sim 40.0 \text{ GHz}$  的频带范围内,吸波器的吸收率均大于  $90\%$ 。而当  $\theta$  增大至  $45^\circ$  时,在  $23.8 \sim 39.3 \text{ GHz}$  的范围内也可实现  $85\%$  以上的宽带吸收率。因此,在 TE 和 TM 极化下,该水基超材料吸波器对宽角入射电磁波都具有良好的吸收效果。

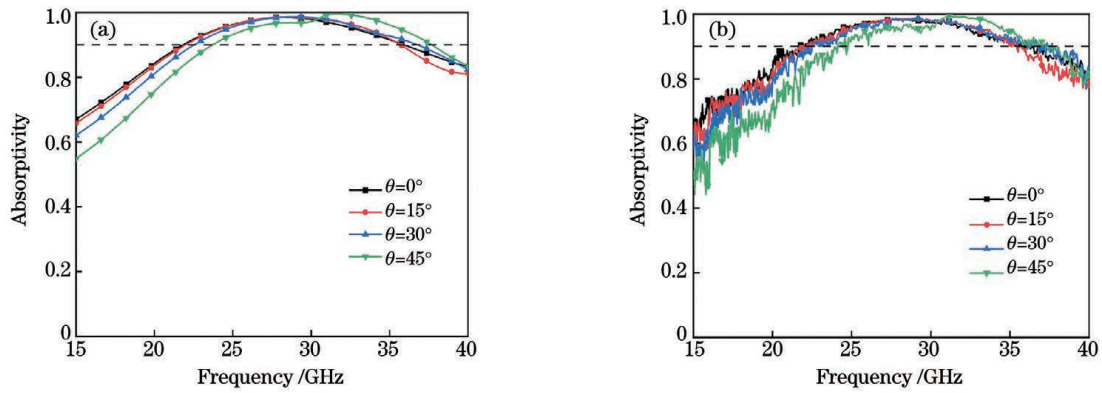


图 9 TE 极化下入射角对吸波体吸收频谱的影响。(a)模拟结果;(b)测试结果

Fig. 9 Effect of incident angle on absorption spectrum of absorber under TE polarization. (a) Simulated results; (b) test results

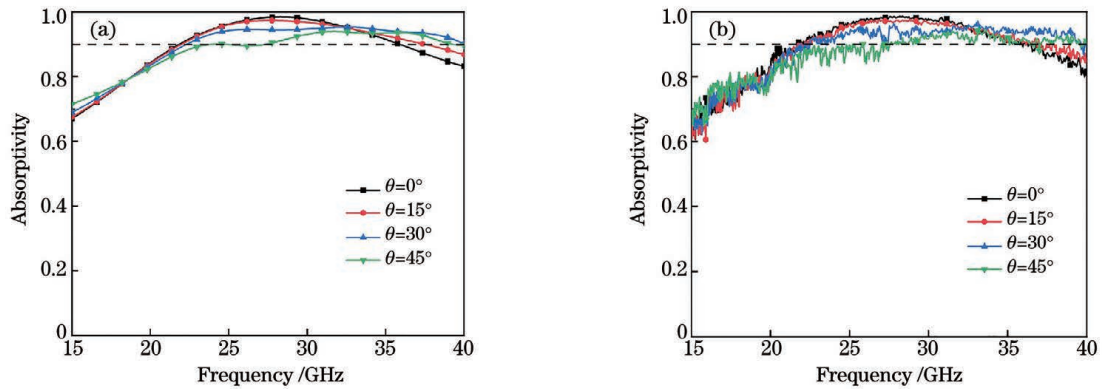


图 10 TM 极化下入射角对吸波体吸收频谱的影响。(a)模拟结果;(b)测试结果

Fig. 10 Effect of incident angle on absorption spectrum of absorber under TM polarization. (a) Simulated results; (b) test results

## 4 结 论

设计了一种基于水介质谐振器的微波吸波器,其谐振单元主要由十字形水腔及其封装结构组成。仿真结果表明,对于 21.8~35.9 GHz 频率范围内的入射波,该吸波器能够实现 90% 以上的吸收率,相对吸收带宽为 48.9%。相比传统水基吸波超材料中互不连通的水基单元,所设计结构中十字形空腔所形成的水流通道横截面面积达到 3 mm×3 mm,可满足吸收器的水冷工作要求,所设计结构可应用于大功率微波吸收场合。此外,所设计结构具有极化无关的吸收特点,在宽角入射情况下也表现出良好的宽带吸收特性。利用 3D 打印技术制作了吸波器样品,并利用自由空间法测试了样品对不同极化角和不同入射角的电磁波的吸收特性,测试结果与仿真结果具有很好的一致性。该研究为大功率电磁波的宽带吸收提供了一种可行的方案。

### 参 考 文 献

[1] 张钰涵,姜文. 现代隐身技术的发展[J]. 电子科技, 2016(3): 194-197.  
Zhang Y H, Jiang W. Development of modern stealth technology [J]. Electronic Science and Technology, 2016(3): 194-197.  
[2] He L H, Deng L W, Luo H, et al. Broadband microwave absorption properties of polyurethane foam absorber optimized

by sandwiched cross-shaped metamaterial[J]. Chinese Physics B, 2018, 27(12): 127801.  
[3] Grant J, Escorcia-Carranza I, Li C, et al. A monolithic resonant terahertz sensor element comprising a metamaterial absorber and micro-bolometer[J]. Laser & Photonics Reviews, 2013, 7(6): 1043-1048.  
[4] Ye D X, Wang Z Y, Xu K W, et al. Ultrawideband dispersion control of a metamaterial surface for perfectly-matched-layer-like absorption[J]. Physical Review Letters, 2013, 111(18): 187402.  
[5] Deng T W, Li Z W, Chua M J, et al. Broadband and ultrathin frequency-dispersive metamaterial screen for reflectivity reduction[J]. IEEE Transactions on Antennas and Propagation, 2015, 63(9): 4156-4160.  
[6] Wu Z, Chen X Q, Zhang Z L, et al. Design and optimization of a flexible water-based microwave absorbing metamaterial[J]. Applied Physics Express, 2019, 12(5): 057003.  
[7] Zhang Z L, Zhang L, Chen X Q, et al. Broadband metamaterial absorber for low-frequency microwave absorption in the S-band and C-band[J]. Journal of Magnetism and Magnetic Materials, 2020, 497: 166075.  
[8] 王超素,江达飞,江孝伟. 偏振无关高吸收效率宽吸收带宽超材料吸收器[J]. 激光与光电子学进展, 2020, 57(3): 031601.  
Wang C S, Jiang D F, Jiang X W. Polarization independent high absorption efficiency wide absorption bandwidth metamaterial absorber[J]. Laser & Optoelectronics Progress, 2020, 57(3): 031601.  
[9] Yahiaoui R, Guillet J P, de Miollis F, et al. Ultra-flexible multiband terahertz metamaterial absorber for conformal geometry applications[J]. Optics Letters, 2013, 38(23): 4988-4990.  
[10] 王杨,轩雪飞,朱路,等. 宽波段高吸收的多层齿轮形超材料吸

- 收器设计[J]. 光学学报, 2021, 41(18): 1823001.
- Wang Y, Xuan X F, Zhu L, et al. Design of multi-layer gear-shaped metamaterial absorber with broadband and high absorption[J]. Acta Optica Sinica, 2021, 41(18): 1823001.
- [11] Ghadimi A, Nayyeri V, Khanjarian M, et al. Design and simulation of a wideband, wide-angle and polarization-insensitive microwave absorber based on pattern optimization of resistive films[J]. Journal of Physics D: Applied Physics, 2021, 54(5): 055102.
- [12] Wang B X, He Y H, Lou P C, et al. Penta-band terahertz light absorber using five localized resonance responses of three patterned resonators[J]. Results in Physics, 2020, 16: 102930.
- [13] Pang Y Q, Cheng H F, Zhou Y J, et al. Ultrathin and broadband high impedance surface absorbers based on metamaterial substrates[J]. Optics Express, 2012, 20(11): 12515-12520.
- [14] Kim Y J, Hwang J S, Yoo Y J, et al. Triple-band metamaterial absorber based on single resonator[J]. Current Applied Physics, 2017, 17(10): 1260-1263.
- [15] Li L Y, Wang J, Ma H, et al. Polarization insensitive metamaterial absorber based on E-shaped all-dielectric structure[J]. Journal of Advanced Dielectrics, 2015, 5(1): 1550009.
- [16] Lu Y, Chen J, Li J X. Design of all-dielectric ultra-wideband transparent water-based absorber[J]. Journal of Physics D: Applied Physics, 2022, 55(11): 115502.
- [17] Zhang H, Ling F, Wang H, et al. A water hybrid graphene metamaterial absorber with broadband absorption[J]. Optics Communications, 2020, 463: 125394.
- [18] Andryieuski A, Kuznetsova S M, Zhukovsky S V, et al. Water: promising opportunities for tunable all-dielectric electromagnetic metamaterials[J]. Scientific Reports, 2015, 5: 13535.
- [19] Zhou Y F, Shen Z Y, Wu J, et al. Design of ultra-wideband and near-unity absorption water-based metamaterial absorber[J]. Applied Physics B, 2020, 126(3): 52.
- [20] Zhao J M, Wei S, Wang C, et al. Broadband microwave absorption utilizing water-based metamaterial structures[J]. Optics Express, 2018, 26(7): 8522-8531.
- [21] Chen J F, Xiao L, Yang J X, et al. Water-based metamaterial absorber applied to ships[C]//2019 International Applied Computational Electromagnetics Society Symposium-China (ACES), August 8-11, 2019, Nanjing, China. New York: IEEE Press, 2019.
- [22] Pang Y Q, Shen Y, Li Y F, et al. Water-based metamaterial absorbers for optical transparency and broadband microwave absorption[J]. Journal of Applied Physics, 2018, 123(15): 155106.
- [23] Xiong H, Yang F. Ultra-broadband and tunable saline water-based absorber in microwave regime[J]. Optics Express, 2020, 28(4): 5306-5316.
- [24] Zhang X F, Zhang D J, Fu Y J, et al. 3-D printed swastika-shaped ultrabroadband water-based microwave absorber[J]. IEEE Antennas and Wireless Propagation Letters, 2020, 19(5): 821-825.
- [25] Lu F T, Han T C. Optically transparent ultra-broadband metamaterial absorber[C]//2019 Photonics & Electromagnetics Research Symposium-Fall (PIERS - Fall), December 17-20, 2019, Xiamen, China. New York: IEEE Press, 2019: 2592-2595.
- [26] Yoo Y J, Ju S, Park S Y, et al. Metamaterial absorber for electromagnetic waves in periodic water droplets[J]. Scientific Reports, 2015, 5: 14018.
- [27] Ellison W J. Permittivity of pure water, at standard atmospheric pressure, over the frequency range 0–25 THz and the temperature range 0–100 °C[J]. Journal of Physical and Chemical Reference Data, 2007, 36(1): 1-18.
- [28] 仇晓琦, 延凤平, 杜雪梅, 等. 角度及温度不敏感的水基宽带超材料吸波器[J]. 中国激光, 2021, 48(16): 1613002.
- Zhang X Q, Yan F P, Du X M, et al. Water-based broadband metamaterial absorber insensitive to angle and temperature[J]. Chinese Journal of Lasers, 2021, 48(16): 1613002.
- [29] 李辉, 余江, 陈哲. 基于混合石墨烯-二氧化钒超材料的太赫兹可调宽带吸收器[J]. 中国激光, 2020, 47(9): 0903001.
- Li H, Yu J, Chen Z. Broadband tunable terahertz absorber based on hybrid graphene-vanadium dioxide metamaterials[J]. Chinese Journal of Lasers, 2020, 47(9): 0903001.

## Broadband High-Power Microwave Absorber Based on Water-Based Metamaterial

Deng Guangsheng<sup>1,2\*</sup>, Chen Wenqing<sup>1</sup>, Yu Zhenchun<sup>1,2</sup>, Yang Jun<sup>1,2</sup>, Yin Zhiping<sup>1,2</sup>

<sup>1</sup>Special Display and Imaging Technology Innovation Center of Anhui Province, Academy of Opto-Electronic Technology, Hefei University of Technology, Hefei 230009, Anhui, China;

<sup>2</sup>Anhui Province Key Laboratory of Measuring Theory and Precision Instrument, School of Instrument Science and Optoelectronics Engineering, Hefei University of Technology, Hefei 230009, Anhui, China

### Abstract

**Objective** Metamaterial microwave absorbers are widely used in many fields, such as radars, stealth technology, electromagnetic compatibility, anti-electromagnetic interference, and sensors. To increase their usability, the functional requirements of absorbers have been also improved, including not only the broadband absorption properties but also wide-angle absorption characteristics. Furthermore, polarization insensitivity is now required, while all-dielectric metamaterials absorbers show unique potential in improving impedance matching in wide band. It is interesting to note that water, as an abundant natural resource on earth, possesses a high dielectric constant and large dispersion, which is of great significance for all-dielectric absorber applications. In addition, most of the water-based absorbers proposed in the literature cannot circulate the aqueous solution between the cells, or the cross-sectional area of the water flow channel of the adjacent cells is too small. The fact that most of the microwave energy absorbed by water-based metamaterials is converted into heat, if the water itself cannot circulate and dissipate heat, indicates the accumulated heat will seriously

deteriorate the working performance of the absorber. However, if a water-based resonant cell with a larger cross-sectional area of the water flow channel is designed, the aqueous solution can be circulated both inside and outside. Hence, the generated heat can be efficiently dissipated during high-power microwave absorption.

**Methods** First, a microwave absorber based on a water-dielectric resonant structure is designed. More specifically, the resonant cell mainly comprises a cruciform water cavity and its respective encapsulation structure. The absorption spectrum of the model is simulated under different polarization angles and incident angles using the finite element method. Moreover, the electromagnetic wave absorption mechanism of the absorber is systematically studied through the distributions of the electric and magnetic fields and power loss density distribution. The array structure consisting  $25 \times 25$  cells is processed by the 3D printing technology. The extracted electromagnetic wave absorption characteristics of the samples under different polarization angles and incident angles are tested using the free space method. Furthermore, the comparison and analysis with the simulated results are performed.

**Results and Discussions** In this study, an all-dielectric water-based microwave absorber is proposed (Fig. 1). The array structure consisting  $25 \times 25$  cells is processed by the 3D printing technology, and the acquired absorption characteristics of the absorber are experimentally investigated by the free space method (Fig. 2). Both the simulated and experimental test results reveal that the absorptivity of the absorber is greater than 90% in the microwave broadband frequency of 21.8–35.9 GHz (Fig. 3). The simulated relative impedances of the water-based absorber are approximately equal to the free space impedance in the operation frequency range, which provides the wideband absorption with high absorptivity (Fig. 4). The electric field, magnetic field, and power loss density at resonant frequency are simulated, and the water layer plays a key role in wideband absorption (Fig. 5). The effects of both the structural parameters and the channel cross-sectional areas on the electromagnetic wave absorption spectrum are also simulated and analyzed (Figs. 6 and 7), and the results provide an important reference for optimizing the structural model. The absorption performances of the absorber at different temperatures are analyzed, and the results suggest that the absorptivity of the absorber is almost insensitive to water temperature changes (Fig. 7). Next, the absorption of the structure at different polarization angles is investigated, and both the simulated and experimental results show that the absorber is insensitive to polarization angles (Fig. 8). Finally, the absorption spectra of the proposed absorber at different incident angles for transverse-electric and transverse-magnetic polarizations are analyzed. The experimental results validate that the structure can maintain wideband absorption at wide incident angle ranges (Figs. 9 and 10).

**Conclusions** A microwave absorber based on a water-dielectric resonator is designed. Simulation results reveal that the absorber can achieve electromagnetic absorptivity of more than 90% in the frequency range of 21.8–35.9 GHz, while the relative absorption bandwidth is 48.9%. Compared with the water-based cells that are not connected to each other in the configuration of the traditional water-based wave-absorbing metamaterials, the cross-sectional area of the water flow channel formed by the cruciform cavity in this structure can reach  $3 \text{ mm} \times 3 \text{ mm}$ . As a result, the water-cooling working condition of the absorber can be addressed, and it can be applied to high-power microwave absorption occasions. In addition, the proposed structure possesses polarization-independent absorption characteristics and also operates well on broadband absorption under wide-angle incidence. The absorber sample is processed by the 3D printing technology, whereas the electromagnetic wave absorption characteristics of the sample under both different polarization and incident angles are explored by the free space method. Interestingly, the test outcomes are in good agreement with the simulation results. Our work therefore provides a practical solution for the enhanced broadband absorption of high-power electromagnetic waves.

**Key words** materials; metamaterial; absorber; broadband; high power; water-based medium